Communications on Applied Nonlinear Analysis
ISSN: 1074-133X
Vol 31 No. 3s (2024)

Two-Dimensional Viscous, Steady, 2-D Nanofluid Flow Past a Permeable Stretching Sheet in Presence of Magnetic Field, Soret and Dufour Effects

Ch. Janaiah[1], G. Upender Reddy[2]

[1]Government Degree College, Sherilingampally, Ranga Reddy District 500 032, Telangana, India(E – Mail:chjohn1505@gmail.com)

ORCID: 0009-0004-5110-9599

[2]Department of Mathematics, Nizam College, Osmania University, Hyderabad – 500 001, Telangana, India(E-Mail: yuviganga@gmail.com)

ORCID: 0009-0008-5075-0279

Article History:

Received: *09-04-2024*

Revised: *21-05-2024*

Accepted: *12-06-2024*

Abstract

This project aims to investigate the interaction between thermal and magnetic fields under stretching conditions. By employing concentration and energy equations, we aim to scrutinize the thermo-diffraction effect. Additionally, we plan to integrate other factors such as fluid injection and suction. Solving boundary layer equations will be facilitated using the Runge-Kutta method. Through graphical representations, we aim to illustrate how various parameters influence temperature, concentration profiles, and velocity. Our findings will be communicated using Sherwood, Nusselt, and skin-friction coefficients. The consistency between our results and previous research underscores the importance of this study in advancing nanotechnology.

Keywords: Thermal Diffusion, Nanofluid, Axi-symmetric flow, linearly stretching sheet, Runge-Kutta Method.

MSC(2020): 35A09, 65L10, 76M20

1. Introduction

The exploration of nanofluids and their impact on thermal conductivity indeed offers a myriad of possibilities across diverse fields. By augmenting the thermal properties of base liquids like water and propylene glycol, engineers can design more efficient cooling systems for electronics, machinery, and even spacecraft [1]. Moreover, the application of nanofluids extends to biomedical realms, where enhanced thermal conductivity can be harnessed for localized cancer therapy, among other medical interventions.

The recent breakthroughs in utilizing solid particles to enhance heat transfer fluids mark a significant advancement [2]. By incorporating solid particles into these fluids, researchers are broadening the scope of materials that can be used for efficient heat transfer applications, potentially leading to more versatile and effective cooling solutions [3]. Boungiorno's research, [4] focusing on Brownian diffusion and the thermophoresis in heat transfer processes, contributes greatly to [5] understanding the underlying mechanisms governing nanofluid behavior. techniques like the control finite volume method enable detailed investigations into natural convection phenomena within nanoporous

materials, offering insights crucial for optimizing heat transfer processes in various engineering applications [6].

Studies by Ganji, Malivandi, [7] and others delve into the intricate interplay between nanoparticle movement and forces in different systems. This research sheds light on the complex dynamics of nanofluid behavior, aiding in the development of predictive models and strategies for manipulating nanofluid properties to achieve desired thermal outcomes. Overall, the collective efforts of researchers like Boungiorno, Ganji, Malivandi,[7] and their peers contribute to advancing our understanding of nanofluid dynamics and unlocking their full potential for a wide range of technological and biomedical applications [8].

Further studies by Mabood and colleagues will look into how radiation, chemical reactions, and dissipation affect the heat transfers and mass of nanofluids. Khan et al., [9] explore dual solutions for hybrid nano-liquids, highlighting the role of nanoparticle volume and concentration in determining thermal conductivity. Studies conducted by Chen and Zhu examine properties [10] of nano-composites and nanowire photodetectors, respectively, contributing to advancements in material science and optoelectronics [11]. Investigations into porous media dynamics reveal insights into processes like fuel cell operation, drying mechanisms, and geothermal energy utilization. The works of Chamkha [12] provide valuable insight into the thermal and mass transfer characteristics of porous materials. New research initiatives [13 – 15] in the area of nanofluidics continue to emerge, unveiling pioneering discoveries. These include the ability to flow nanofluids over stretched surfaces without the effects of thermal radiation [16 - 28].

Ongoing projects aim to explore the effects of Casson fluid dynamics on stretched sheets under various influences, with boundary layer equations adapted for numerical solutions using methods like Runge-Kutta–Fehlberg combined with shooting techniques. Graphical representations of temperature, mass transfer rates, nanoparticle concentration, and skin-friction coefficients provide visual insights into the multifaceted behaviors of nanofluids in different dimensions.

2. Mathematical formulation

This research project aims to examine the distribution of two-dimensional stagnation points within a nanofluid system, where the presence of Dufour and Soret thermal diffusion effects is notable.

The physical coordinates of this material are aligned with the longitudinal axis of a stretching sheet.

Key assumptions and boundary conditions include: h_f, $u_w(x) = ax$ $(B = B_o)$

i. Convective heating occurs on the sheet's lower surface. The temperature at which this occurs is referred to as (T_f).
ii. The nanoparticle concentration and ambient temperature remain uniform. The two are represented by $T_\infty$and C_∞ .
iii. Conductivity and incompressibility are the properties of the fluid.
iv. The nanoparticle flux does not occur at the surface. The boundary condition also contributes to thermophoresis effects.
v. The surface of the sheet maintains its constant stretching velocity.

vi. A magnetic field perpendicular to the flow surface is introduced, with its strength considered negligible due to its relatively small magnitude.

vii. The assumption is made that thermal equilibrium is established between the base fluid and the suspended particles.

viii. The rheological equation for a non-Newtonian fluid is defined as,

$$\tau = \tau_o + \mu\alpha^* \tag{1}$$

ix. Eq. (1) can be expanded for Casson fluid as,

$$\tau_{ij} = \begin{cases} 2\left(\mu_B + \dfrac{p_y}{\sqrt{2\pi}}\right)e_{ij}, & \pi > \pi_c \\ 2\left(\mu_B + \dfrac{p_y}{\sqrt{2\pi_c}}\right)e_{ij}, & \pi < \pi_c \end{cases} \tag{2}$$

where $\pi = e_{ij}e_{ji}$ with e_{ij} is the $(i,\ j)^{th}$ component of fluid deformation rate and $p_y = \dfrac{\mu_B\sqrt{2\pi}}{\beta}$ is the yield stress of the Casson fluid.

The governing equations for mass, energy, and momentum of nanoparticles are formulated based on boundary layer assumptions and approximations derived from previous studies on stretching magnetic fields.

Continuity Equation

$$\left(\frac{\partial u}{\partial x}\right)+\left(\frac{\partial v}{\partial y}\right)=0 \tag{3}$$

Momentum Equation

$$u\left(\frac{\partial u}{\partial x}\right)+v\left(\frac{\partial u}{\partial y}\right)=\nu\left(1+\frac{1}{\beta}\right)\left(\frac{\partial^2 u}{\partial y^2}\right)+U_\infty\left(\frac{\partial U_\infty}{\partial x}\right)-\left(\frac{\sigma B_o^2}{\rho_f}\right)\left(u-U_\infty\right)-\frac{\nu}{K}\left(u-U_\infty\right) \tag{4}$$

Equation of thermal energy

$$u\left(\frac{\partial T}{\partial x}\right)+v\left(\frac{\partial T}{\partial y}\right)=\alpha\left(\frac{\partial^2 T}{\partial y^2}\right)+\frac{(\rho C)_p}{(\rho C)_f}\left\{D_B\left[\frac{\partial C}{\partial y}\frac{\partial T}{\partial y}\right]+\frac{D_T}{T_\infty}\left[\frac{\partial T}{\partial y}\right]^2\right\} \tag{5}$$

Equation of species nanoparticle concentration

$$u\left(\frac{\partial C}{\partial x}\right)+v\left(\frac{\partial C}{\partial y}\right)=D_B\left(\frac{\partial^2 C}{\partial y^2}\right)+\frac{D_T}{T_\infty}\left(\frac{\partial^2 T}{\partial y^2}\right) \tag{6}$$

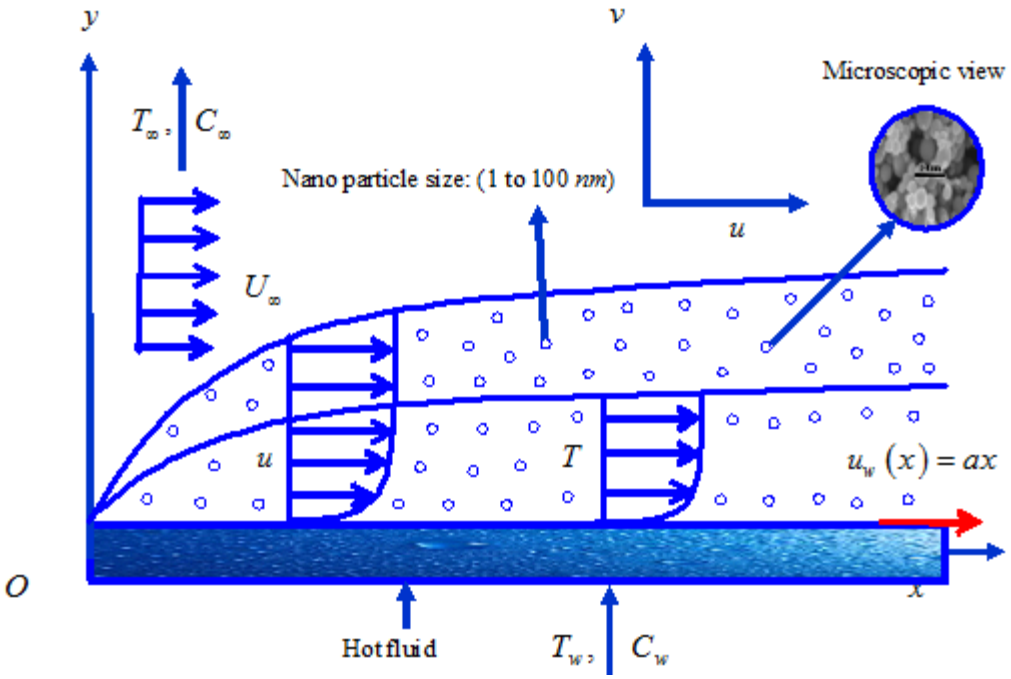

Figure 1: Geometry representation of the fluid

The boundary conditions for nano-fluid flow are

$$\left.\begin{aligned} &u = u_w(x) = ax,\ v = 0,\ -\kappa\left(\frac{\partial T}{\partial y}\right) = h_f\left(T_f - T\right),\ D_B\left(\frac{\partial C}{\partial y}\right) + \frac{D_B}{T_\infty}\left(\frac{\partial T}{\partial y}\right) = 0 \ at\ \ y = 0 \\ &u \to U_\infty = bx,\ v = 0,\ T \to T_\infty,\ C \to C_\infty \ as\ \ y \to \infty \end{aligned}\right\} \quad (7)$$

For solving governing equations (4), (5) and (6), the following similarity variables are introduced

$$\left.\eta = y\sqrt{\frac{a}{\nu}},\ \psi = xf(\eta)\sqrt{a\nu},\ \theta = \frac{T - T_\infty}{T_f - T_\infty},\ \phi = \frac{C - C_\infty}{C_\infty}\right\} \quad (8)$$

where $\psi(x, y)$represents the stream function is given as

$$u = \frac{\partial \psi}{\partial y} \text{ and } v = -\frac{\partial \psi}{\partial x} \quad (9)$$

Using Eq. (8), the fundamental Eqs. (4) to (6) become

$$\left(1 + \frac{1}{\beta}\right) f''' + ff'' - f'^2 + A^2 + (M + \Omega)(A - f') = 0 \quad (10)$$

$$\theta'' + \Pr f\theta' + \Pr Nb\theta'\phi' + \Pr Nt\theta'^2 = 0 \quad (11)$$

$$Nb\phi'' + LeNb \Pr f\phi' + Nt\theta'' = 0 \quad (12)$$

and the corresponding boundary conditions will (7) become

$$\left.\begin{aligned} &f = 0,\ f' = 1,\ \theta' = Bi(\theta - 1), Nb\,\phi' + Nt\theta' = 0 \ at\ \eta = 0 \\ &f' \to A,\ \theta \to 0,\ \phi \to 0 \ as\ \eta \to \infty \end{aligned}\right\} \quad (13)$$

where involved physical parameters are defined as

$$\left.\begin{aligned} &Bi=\frac{h_f}{\kappa}\sqrt{\frac{\nu}{a}},\ \Pr=\frac{\nu}{\alpha},\ A=\frac{b}{a},\ Le=\frac{\alpha}{D_B},\ M=\frac{\sigma B_o^2}{\rho_f a},\\ &\Omega=\frac{\nu}{Ka},\ Nb=\frac{(\rho C)_p D_B C_\infty}{\nu(\rho C)_f},\ Nt=\frac{(\rho C)_p D_T(T_f-T_\infty)}{\nu T_\infty(\rho C)_f}\end{aligned}\right\} \tag{14}$$

The physical parameters of interest, namely the skin-friction coefficient (Cf) and local Nusselt number (Nu_x), are presented as follows:

$$Cf=\left(1+\frac{1}{\beta}\right)\frac{\tau_w}{\rho u_w^2}\Rightarrow \mathrm{Re}_x^{-\frac{1}{2}}Cf=-\left(1+\frac{1}{\beta}\right)f''(0)\ \text{ where }\ \tau_w=\mu\left(\frac{\partial u}{\partial y}\right)_{y=0} \tag{15}$$

$$Nu_x=\frac{xq_w}{\kappa\left(T_f-T_\infty\right)}\ \text{ where }\ q_w=-\kappa\left(\frac{\partial T}{\partial y}\right)_{y=0}\Rightarrow \mathrm{Re}_x^{-\frac{1}{2}}Nu_x=-\theta'(0) \tag{16}$$

$$Sh_x=\frac{q_m x}{D_B\left(C_w-C_\infty\right)}\ \text{ where }\ q_m=-D_B\left(\frac{\partial C}{\partial y}\right)_{y=0}\Rightarrow \mathrm{Re}_x^{-\frac{1}{2}}Sh_x=-\phi'(0) \tag{17}$$

where $\mathrm{Re}_x=\frac{ax^2}{\nu}$ be a local Reynolds number.

3. Method of Solution

The first and second conditions of a differential equation can be specified with the addition of an unconstrained domain. This method can be used to numerically calculate the solution.The first-order boundary value problems of (10)-(12) are characterized by a nonlinear relationship between the third and second-order integral ODEs. The first set of problems is then whittled down to seven to reveal unknown issues arising from a particular assumption or method.

$$\left.f=y_1,\ f'=y_2,\ f''=y_3,\ \theta=y_4,\ \theta'=y_5,\ \phi=y_6,\ \phi'=y_7\right\} \tag{18}$$

The Rung-kutta method is often utilized to solve systems with mismatched initial conditions. It involves performing tests to find suitable boundary conditions while also guessing the missing ones.To ensure that the results are accurate, the step sizes are set at 0.001. This ensures that the solution's granularity is precisely determined.

4. Program Code Validation

The numerical approach used for the study was analyzed to ensure that it was comparable to the previous information. The results support [29] Ibrahim and Ishak's assertions [30]. Table-2 reveals different numerical values for Pr, while ignoring the effects of Thermophoresis and Nb. The findings of the study support the assertions made by [31] Gupta, Mahapatra, Hayat, and Ibrahim [32]. They demonstrate the high degree of confidence in the current numerical code's reliability [33]. Table-1 and Table-2 show the level of concurrence exhibited by the study's findings.

A	Ibrahim et al. [30]	Ishak et al. [32]	Present Results
0.1	0.9684	0.9689	0.9536652145
0.2	0.9181	0.9185	0.9055022780
0.5	0.6672	0.6671	0.6533840182
2.0	2.0171	2.0172	2.0083364532
3.0	4.7293	4.7295	4.7118566334

Table 1: Comparison of the Skin-friction coefficient $-f''(0)$ results for different values of A when $M = \beta = \Omega = 0$

Pr	A	Ibrahim et al. [30]	Mahapatra and Gupta [31]	Hayat et al. [32]	Present results
1.0	0.1	0.6022	0.6030	0.602156	0.5822301544
	0.2	0.6245	0.6250	0.624467	0.6103557847
	0.5	0.6924	0.6920	0.692460	0.6823304712
1.5	0.1	0.7768	0.7770	0.776802	0.7682216630
	0.2	0.7971	0.7970	0.797122	0.7854430224
	0.5	0.8648	0.8630	0.864771	0.8532290445

Table 2: Results of the comparison of the Nusselt number with different values are Pr and A when $Nb = Nt = 0$

5. Results and Discussions

This section covers the various parameters of nanoparticles that affect their temperature, concentration, and velocity profiles. Table 3, 4, and 5 show the coefficients of mass transfer, heat transfer, and skin friction.

The flow, mass, and thermal attributes of a system are shown in the tables and figures

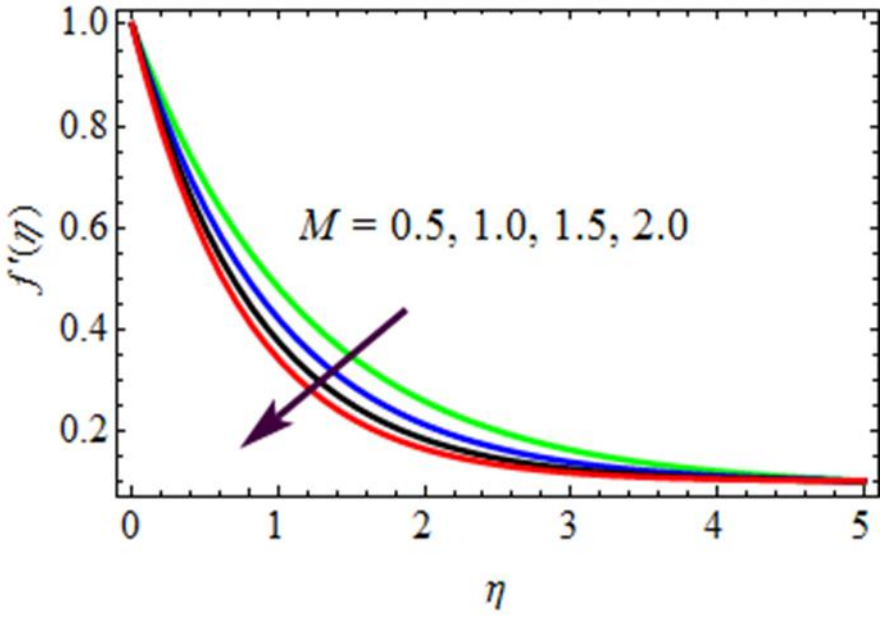

Figure 2: Influence of M on velocity profiles

The velocity profiles' effects on the M parameter is shown in Figure 2. An increase in values can shrink profiles, which leads to a magnetic force with a stronger strength. This also affects thermal boundary layers and momentum. On the other, a Lorentz Force's strength can make the thermal boundary layer thicker.

The Lorentz force is a type of resistance or opposing force caused by a magnetic field. It can affect the thickness and velocity of fluids. This concept shows how the M parameter can affect the attributes of a system's flow.

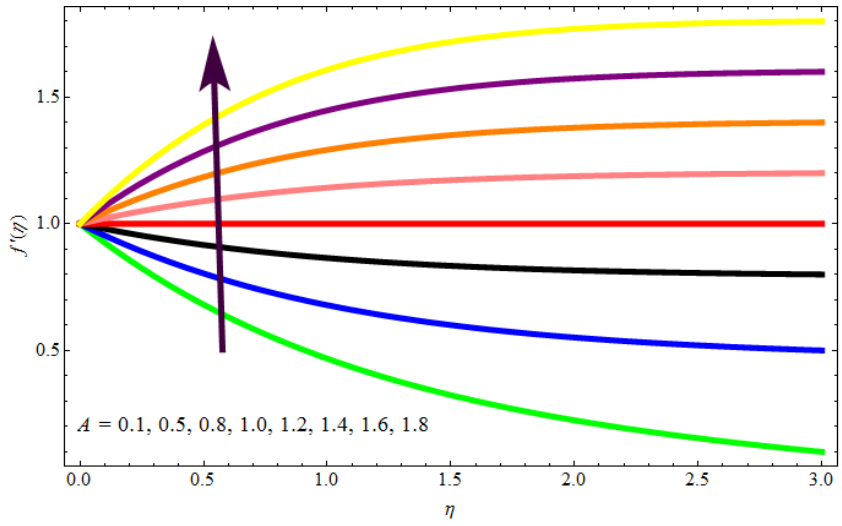

Figure 3: Influence of A on velocity profiles

Figure 3 depicts the velocity profiles for different values of parameter A. It is evident from the graph that as the velocity increases, the boundary layer thickness also grows.

Under specific conditions, the flow velocity can be augmented. The graph elucidates how parameter A affects the behaviour of the boundary layer.

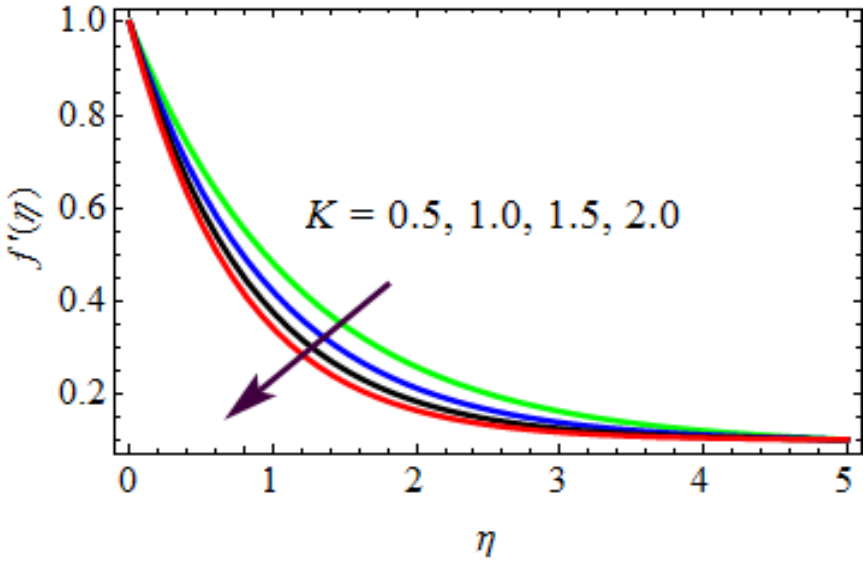

Figure 4: Influence of K on velocity profiles

The velocity distribution shown in Figure 4 is the result of Permeability's changes in parameters. The K 's magnifies the thickness of a porous layer, which then decreases its velocity.

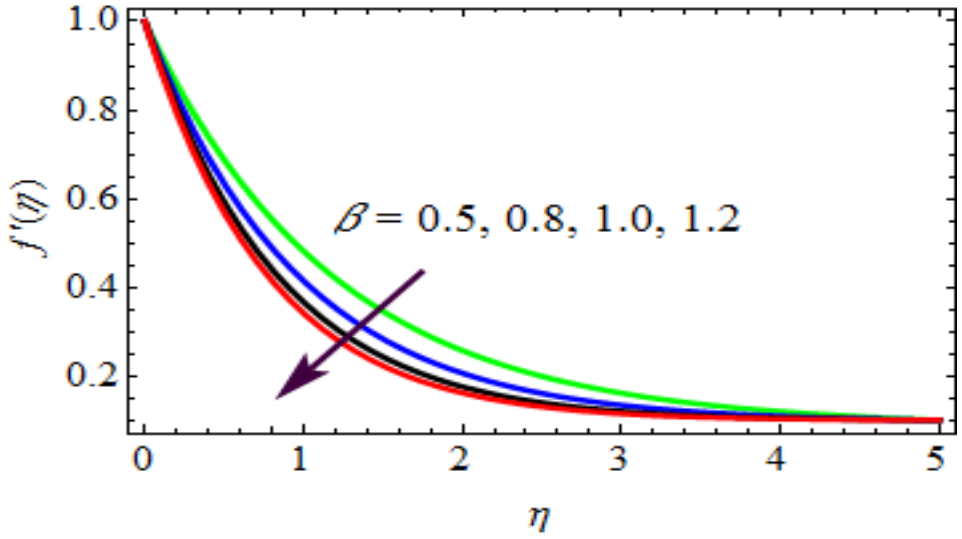

Figure 5: Influence of β on velocity profiles

The velocity profiles of many types of fluids as shown in Figure 5.And Casson factor's increase can have an impact on the profile of the boundary layer. A graph shows how similar its behavior is to that of Newtonian fluids.

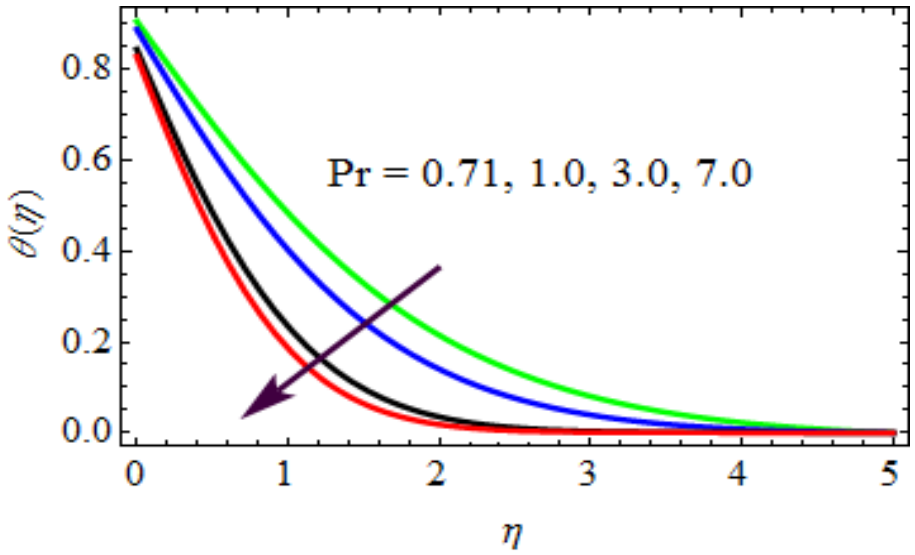

Figure 6: Influence of Pr on velocity profiles

The thermal properties of certain Prandtl numerals show that their increasing number significantly decreases their thickness. This suggests that the heat diffuses in bigger fluid bodies, which can lead to an increase in thermal diffusivities.

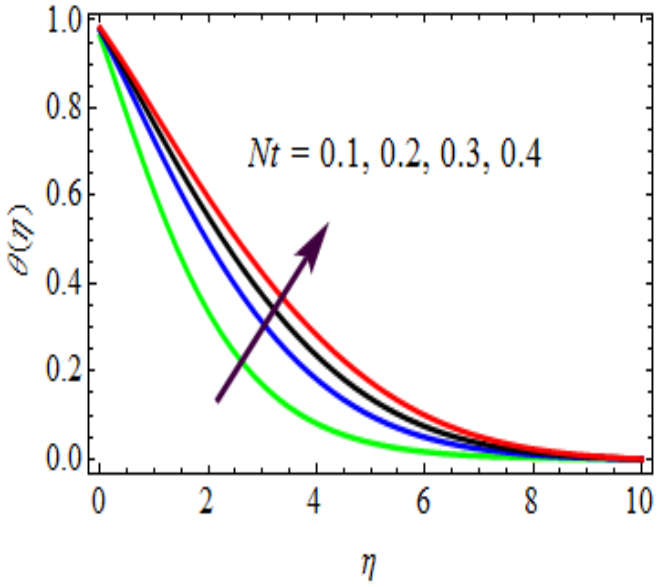

Figure 7: Influence of Nt on temperature profiles

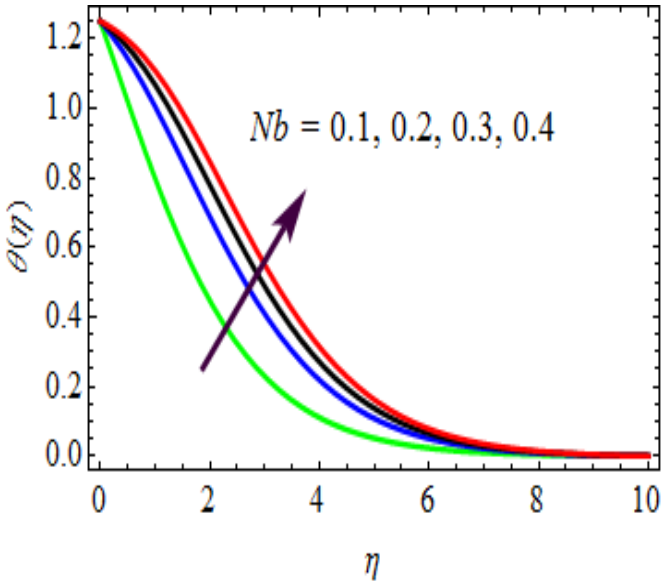

Figure 8: Influence of Nb on temperature profiles

Figure 7 illustrates the impact of *Nt* and *Nb* thermophoresis on the thermal profiling of a region. The utilization of these factors leads to elevated temperature levels and distinctive thermal boundary layer behavior. Furthermore, an increase in thermophoretic force enhances the region's profile.

In comparison to non-Newtonian fluids, Newtonian fluids exhibit a higher thermal profile. Additionally, the Brownian motion parameter aids in heating the physical setup of the region, facilitating the transfer of nanoparticles from the cold stretch sheet region to its quiescent fluid zone.

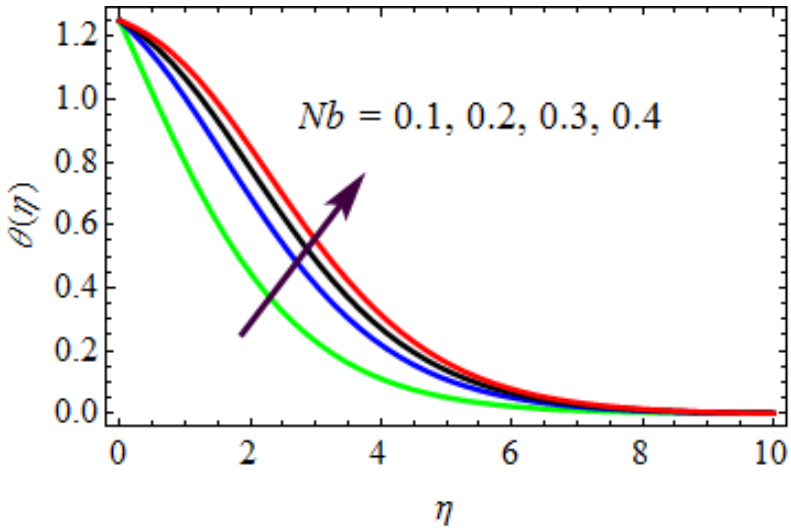

Figure 9: The concentration profiles of nanoparticles are affected by *Nb*

The increment in the *Nb* parameter in Figure 9 had the significant effect on the nano-liquidity function. The data collected through a physical analysis revealed that the collision between fluids has an impact on the nanoparticle's concentration.

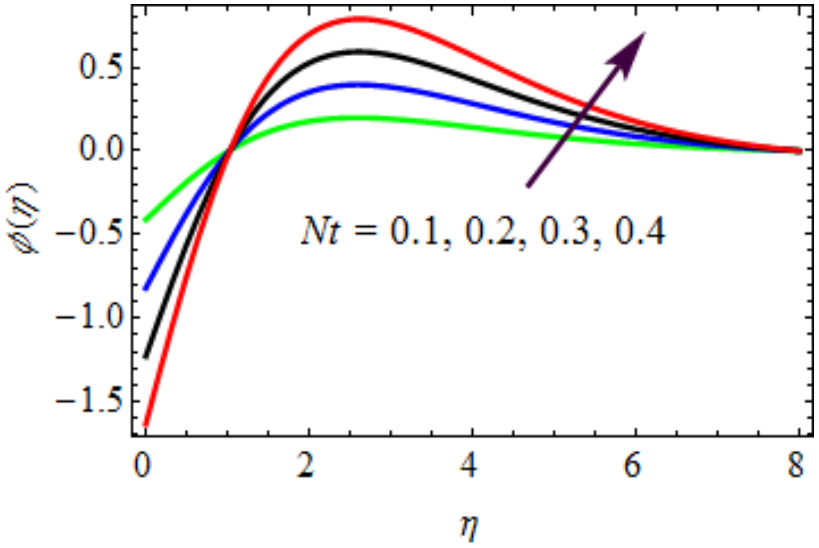

Figure 10: Influence of Nt on nanoparticle concentration profiles

Figure 10 shows how the Thermophoresis function affects the nanoparticle concentration profiles. The difference between the two is that the former's motion gradient counteracts the latter, causing a reduction in the nanoparticles' surface concentration profile.

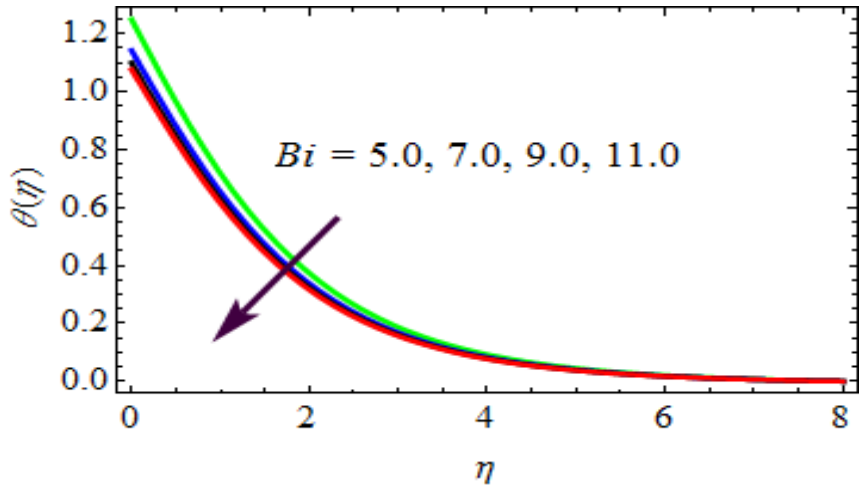

Figure 11: Influence of the Bi on temperature profiles

The Biot number shows the thermal profile of the body when it's exposed to convection heat. It indicates how heat flows through the surface as it increases in temperature.

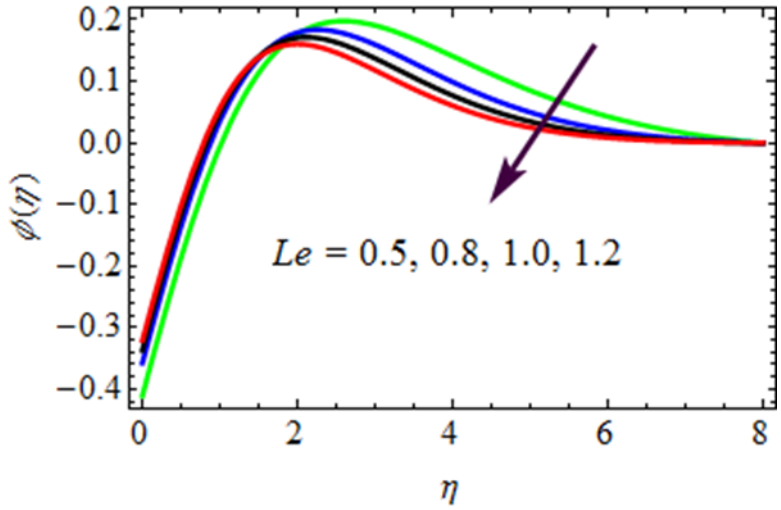

Figure 12: Influence of *Le* on nanoparticle concentration profiles

The reduction in the distribution of nanoparticles shown in Figure 12 is attributed to the Lewis number formula. The lower the number, the greater it is, and the lower it is dependent on the Brownian diffusion coefficient.

A	*M*	Pr	*Nt*	*Nb*	*K*	*Bi*	*Le*	*Cf*
0.2	0.5	0.71	0.1	0.1	0.5	5.0	0.1	1.0822160251
0.4								1.1250028897
0.8								1.1593302487
1.0								1.1735590143
	0.8							0.9877521566
	1.0							0.9682210433
	1.2							0.9422501551
		1.0						1.0622015234
		3.0						0.9721560329
		7.0						0.9632250154
			0.2					1.1326005482
			0.3					1.1596620144
			0.4					1.1620034218
				0.2				1.1482005166
				0.3				1.1693320475
				0.4				1.1782205446
					1.0			1.0682215468
					1.5			1.0235117852
					2.0			1.0032600154
						7.0		1.1566288421
						9.0		1.1892201560
						11.0		1.2082230542
							0.2	1.0450362185
							0.3	1.0260052132
							0.4	0.9852201506

Table-3.: The value of variations in the coefficient of skin friction can be used to forecast future changes .of A, M, Pr, Nt, Nb, K, Bi and Le

The table below shows the various compounds' Nusselt numbers and their heat transfer coefficient. It shows that their varying values can increase the coefficient's rate. On the other hand, when the Pr's values go up, the opposite occurs.

Table-4 illustrates the influence that compounds such as Nt, Bi, and Nb had on the heat transfer's rate. The increases in these compounds, which can be attributed to certain processes, such as Brownian motion and thermophoresis, speeds up the transfer. On the other hand, the increase in Pr reduces the speed of the process. This suggests that the higher Prandtl values lead to a decrease in thermal conductivity.

Pr	Nt	Nb	Bi	Nu_x
0.71	0.1	0.1	5.0	0.7052213568
1.0				0.6482265179
3.0				0.6023352015
7.0				0.5893320144
	0.2			0.7782254969
	0.3			0.7966201554
	0.4			0.8023301546
		0.2		0.7863221405
		0.3		0.8012550422
		0.4		0.8162290488
			7.0	0.7293360041
			9.0	0.7395543001
			11.0	0.7482201556

Table-4.: Rate of heat transfer coefficient values for different values of Pr, Nt, Nb and Bi

The table below illustrates the varying effects of Nt, Nb and Le on the Sherwood factor. As their values increase, the Sherwood number factor falls. The mass transfer rate can be affected by various factors, such as thermophoresis and the Brownian motion. The higher the value of Nb and Nt the more powerful the dispersion and particle migration effects are. On the contrary, the increase in the Lewis number can make the process less efficient. The table below illustrates the varying impacts of Nt, Le and Nb on the mass transfer rate. It also shows their role in the computation.

Nt	Nb	Le	Sh_x
0.1	0.1	0.1	0.9122502365
0.2			0.8723306654
0.3			0.8520015711
0.4			0.8320062945
	0.2		0.8802115474
	0.3		0.9032201622
	0.4		0.9233105448
		0.2	0.8720015302
		0.3	0.8210050214
		0.4	0.8032006215

Table-5.: Rate of mass transfer coefficient values for different values of Nt, Nb and Le

6. Conclusions

We have investigated the numerical solutions of concentration, velocity and temperature profiles of steady nanofluid flow over a stretching sheet. The effects of the Dufour, Soret and Magnetic field are also incorporated in this research work. It is found that for a particular set of engineering parameters, the skin-friction coefficient and the local Sherwood and Nusselt numbers are demonstrate numerical solutions over a broad region of steadiness parameter. The final results are concluded as follows:

- The resultant velocity profiles are dropping through an increase in Magnetic field parameter, Suction/Injection parameter and Stretching sheet parameter.
- The resultant temperature profiles are increased with an increase in Thermophoresis, Brownian motion, Dufour number and reverse effect is observed with Prandtl number.
- Species concentration of nanofluid is decreased with an increase in Lewis number, Brownian motion parameter and the opposite effect is observed in case of Thermophoresis and Soret number parameters.
- In program code validation, the obtained results are in good agreement with the published results.
- The present problem has more applications through magnetic materials processing, electrically conducting polymer dynamics, and purification of molten metal by non-metallic.
- This study may be prolonged for Maxwell and Jeffrey nanofluids, the non-Newtonian nature of blood flow through the constricted vein of the elliptical cross-section, and some other types of non-Newtonian nanofluids subject to various physical conditions.

Nomenclature

f : Dimensionless stream function
u, w: Velocity components in r and z axes respectively (m/s)
r, z: Cylindrical coordinates measured along the stretching sheet (m)
f' : Fluid velocity (m/s)
Du : Diffusion thermo (or) Dufour number
Pr : Prandtl number
Sr : Thermal diffusion (or) Soret number
C_∞ : Dimensional ambient volume fraction $\left(mol/m^3\right)$
C : Fluid concentration $\left(mol/m^3\right)$
T_w : Temperature at the surface $\left(K\right)$
T : Fluid temperature $\left(K\right)$
O : Origin
M : Magnetic field parameter
Cf : Skin-friction coefficient
T_∞ : Temperature of the fluid far away from the stretching sheet $\left(K\right)$
Nu_x: Rate of heat transfer coefficient (or) Nusselt number
B_o : Uniform magnetic field
T_m : Fluid Mean temperature

C_p : Specific heat at constant pressure
C_f : Specific heat capacity of base fluid
C_s : Concentration susceptibility
D_m : Solutal diffusivity of the medium
K_T : Thermal diffusion ratio
Nb : Brownian motion parameter
Sc : Schmidt number
D_B : Thermophoresis diffusion coefficient
D_T : Brownian diffusion coefficient
a : A constant parameter
u_w : Wall velocity along the *r*-coordinate (*m*/*s*)
Nt : Thermophoresis parameter
Re_r : Reynold's number
n : Power-law index parameter

Greek symbols:

ϕ : Dimensional concentration $\left(mol/m^3\right)$
θ : Dimensionless temperature $\left(K\right)$
η : Dimensionless similarity variable
α : Thermal diffusivity $\left(m^2/s\right)$
ν_f : Kinematic viscosity $\left(m^2/s\right)$
μ : Dynamic viscosity of the fluid
σ : Electrical Conductivity
κ : Thermal conductivity of the fluid
ψ : Stream function
ρ_f : Density of the base fluid
ρ_p : Density of nano-fluid

Superscript:

$/$: Differentiation w.r.t η

Subscripts:

w : Condition on the sheet
f : Fluid
∞ : Ambient Conditions

Competing Interests

The authors declare that they have no competing interests

References

[1] J. Boungiorno, Convective transport in nanofluids, J. Heat Tran., 128 (2006), 240-250, https://doi.org/10.1115/1.2150834.

[2] M. Sheikholeslami, M. Gorji-Bandpy, D. D. Ganji and S. Soleimani, Effect of a magnetic field on natural convection in an inclined half-annulus enclosure filled with Cu-water nanofluid using CVFEM, Adv. Powder Technol., 24 (2013), 980-991, https://doi.org/10.1016/j.apt.2013.01.012.

[3] A. Malvandi and D. D. Ganji, Effects of nanoparticle migration on force convection of alumina/water nanofluid in a cooled parallel-plate channel, Adv. Powder Technol., 25 (2014), 1369-1375, https://doi.org/10.1016/j.apt.2014.03.017.

[4] A. A. Servati, K. Javaherdeh and H. R. Ashorynejad, Magnetic field effects on force convection flow of a nanofluid in a channel partially filled with porous media using lattice Boltzmann method, Adv. Powder Technol., 25 (2014), 666-675, https://doi.org/10.1016/j.apt.2013.10.012.

[5] Khalil Khanafer and KambizVafai, A critical synthesis of thermophysical characteristics nanofluids, Int. J. Heat Mass Transfer, 54 (2011), 4410-4428, https://doi.org/10.1016/j.ijheatmasstransfer.2011.04.048.

[6] F. Mabood, S. Shateyi, M. M. Rashidi, E. Momoniat and N. Freidoonimehr, MHD stagnation point low heat and mass transfer of nanofluids in porous medium with radiation, viscous dissipation and chemical reaction, Advanced Powder Technology, 27(2) (2016),742-749, https://doi.org/10.1016/j.apt.2016.02.033.

[7] Yi-Xia Li, Mohammed Hamed Alshbool, Yu-Pei Lv, Ilyas Khan, M. Riaz Khan and AlibekIssakhov, Heat and mass transfer in MHD Williamson nanofluid flow over an exponentially porous stretching surface, Case Studies in Thermal Engineering, 26 (2021), 100975, https://doi.org/10.1016/j.csite.2021.100975.

[8] A. V. Kuznetsov and D.A. Nield, Natural convective boundary-layer flow of a nanofluid past a vertical plate, Int. J. Therm. Sci., 49 (2) (2010), 243-247, https://doi.org/10.1016/j.ijthermalsci.2009.07.015.

[9] D. A. Nield and A. V. Kuznetsov, The Cheng–Minkowycz problem for natural convective boundary-layer flow in a porous medium saturated by a nanofluid, Int. J. Heat Mass Transf., 52(25-26) (2009), 5792 -5795, https://doi.org/10.1016/j.ijheatmasstransfer.2013.06.054.

[10] S. Chen, M. K. Hassanzadeh-Aghdam and R. Ansari, An analytical model for elastic modulus calculation of SiC whisker-reinforced hybrid metal matrix nanocomposite containing n-SiC nanoparticles, J. Alloys Compd., 767 (2018), 632-641, https://doi.org/10.1016/j.jallcom.2018.07.102.

[11] X. Zhu, F. Lin, Z. Zhang, X. Chen, H. Huang, D. Wang and Z. Wei, Enhancing performance of a GaAs/AlGaAs/GaAs nanowire photodetector based on the two-dimensional electron-hole tube structure, Nano Lett., 20(4) (2020), 2654-2659, DOI: 10.1109/ICOEI51242.2021.9453040.

[12] A. J. Chamkha, C. Issa and K. Khanafer, Natural convection from an inclined plate embedded in a variable porosity porous medium due to solar radiation, Int. J. Therm. Sci., 41(1) (2002), 73-81, https://doi.org/10.1016/S1290-0729(01)01305-9.

[13] N. Hadidi, R. Bennacer and Y. Ould-Amer, Two-dimensional thermosolutal natural convective heat and mass transfer in a bi-layered and inclined porous enclosure, Energy, 93 (2015), 2582-2592, https://doi.org/10.1016/j.energy.2015.10.121.

[14] W. A. Khan, J. R. Culham and O. D. Makinde, Combined heat and mass transfer of third grade nanofluids over a convectively heated stretching permeable surface, Can. J. Chem. Eng., 93(10) (2015), 1880-1888, https://doi.org/10.1002/cjce.22283.

[15] N. Freidoonimehr, M. M. Rashidi and S. Mahmud, Unsteady MHD free convective flow past a permeable stretching vertical surface in a nano-fluid, Int. J. Therm. Sci., 87 (2015), 136-145, https://doi.org/10.1016/j.ijthermalsci.2014.08.009.

[16] Z. Abdelmalek, T. Tayebi, A. S. Dogonchi, A. J. Chamkha, D. D. Ganji and I. Tlili, Role of various configurations of a wavy circular heater on convective heat transfer within an enclosure filled with nanofluid, Int. Commun. Heat Mass Transf., 113, (2020), 104525, https://doi.org/10.1016/j.icheatmasstransfer.2020.104525.

[17] T. Tayebi and A. J. Chamkha, Entropy generation analysis due to MHD natural convection flow in a cavity occupied with hybrid nanofluid and equipped with a conducting hollow cylinder. J. Therm. Anal. Calorim., 139 (2020), 2165-2179, https://doi.org/10.1007/s10973-019-08651-5.

[18] T. Tayebi and A. J. Chamkha, Entropy generation analysis during MHD natural convection flow of hybrid nanofluid in a square cavity containing a corrugated conducting block, Int. J. Numer. Methods Heat & Fluid Flow, 30(3) (2020), 1115-1136, https://doi.org/10.1108/HFF-04-2019-0350.

[19] D. Toghraie, R. Mashayekhi, H. Arasteh, H., S. Sheykhi, M. Niknejadi and A. J. Chamkha, Two-phase investigation of water-Al2O3 nano-fluid in a micro concentric annulus under non-uniform heat flux boundary conditions", Int. J. Numer. Methods Heat & Fluid Flow, 30(4), (2020), 1795-1814, https://doi.org/10.1108/HFF-11-2018-0628.

[20] A. J. Chamkha, A. S. Dogonchi and D. D. Ganji, Magneto-hydrodynamic flow and heat transfer of a hybrid nanofluid in a rotating system among two surfaces in the presence of thermal radiation and Joule heating, AIP Adv., 9, 025103 (2019), https://doi.org/10.1063/1.5086247.

[21] J. Raza, F. Mebarek-Oudina and A. J. Chamkha, Magnetohydrodynamic flow of molybdenum disulfide nano-fluid in a channel with shape effects", Multidiscipline Modeling in Materials and Structures, 15(4), (2019), 737-757, https://doi.org/10.1108/MMMS-07-2018-0133.

[22] N. S. Shashikumar, B. J. Gireesha, B. Mahanthesh, B. C. Prasannakumara and A. J. Chamkha, Entropy generation analysis of magneto-nanoliquids embedded with aluminium and titanium alloy nanoparticles in microchannel with partial slips and convective conditions, Int. J. Numer. Methods for Heat & Fluid Flow, 29(10), (2019), 3638-3658, https://doi.org/10.1108/HFF-06-2018-0301.

[23] M. Veera Krishna and A. J. Chamkha, Hall and ion slip effects on MHD rotating boundary layer flow of nanofluid past an infinite vertical plate embedded in a porous medium, Results Phy., 15, (2019), 102652, https://doi.org/10.1016/j.rinp.2019.102652

[24] A. J. Chamkha and M. Djezzar, Natural convection of CNT-water nano fluid in an annular space between confocal elliptic cylinders with constant heat flux on inner wall,Scientia Iranica, 26(5 (Transactions B: Mechanical Engineering)), (2019), 2770-2783, DOI:10.24200/SCI.2018.21069.

[25] A. I. Alsabery, R. Mohebbi, A. J. Chamkha, I. Hashim, Effect of local thermal non-equilibrium model on natural convection in a nanofluid-filled wavy-walled porous cavity containing inner solid cylinder, Chem. Eng. Sci., 201, (2019), 247-263, https://doi.org/10.1016/j.ces.2019.03.006.

[26] S. Izadi, T. Armaghani, R. Ghasemias, A. J. Chamkha and M. Molana, A comprehensive review on mixed convection of nano-fluids in various shapes of enclosures, Powder Technol., 343, (2019), 880-907, https://doi.org/10.1016/j.powtec.2018.11.006.

[27] P. Sudarsana Reddy, P. Sreedevi and A. J. Chamkha, MHD boundary layer flow, heat and mass transfer analysis over a rotating disk through porous medium saturated by Cu-water and Ag-water nanofluid with chemical reaction, Powder Tech., 307, (2017), 46-55, https://doi.org/10.1016/j.powtec.2016.11.017.

[28] F. Selimefendigil, M. A. Ismael and A. J. Chamkha, Mixed convection in superposed nanofluid and porous layers in square enclosure with inner rotating cylinder, Int. J. Mech. Sci., 124–125, 2017, 95-108, https://doi.org/10.1016/j.ijmecsci.2017.03.007.

[29] A. S. Dogonchi, T. Tayebi and A. J. Chamkha, Natural convection analysis in a square enclosure with a wavy circular heater under magnetic field and nanoparticles, J. Therm. Anal. Calorim., 139, (2020), 661-671, https://doi.org/10.1007/s10973-019-08408-0.

[30] W. Ibrahim, B. Shankar and M. M. Mahantesh, MHD stagnation point flow and heat transfer due to nanofluid towards a stretching sheet, Int. J. Heat Mass Transf., 56, (2013), 1-9, , https://doi.org/10.1016/j.ijheatmasstransfer.2012.08.034.

[31] T. R. Mahapatra and A. G. Gupta, Heat transfer instagnation point flow towards a stretching sheet, Heat Mass Transf., 38, (2002), 517-521, DOI:10.1007/s002310100215.

[32] A. Ishak, R. Nazar and I. Pop, Mixed convection boundary layers in the stagnation point flow towards a stretching vertical sheet, Meccanica, 41, (2006), 509-518, https://doi.org/10.1007/s11012-006-0009-4.

[33] T. Hayat, M. Mustafa, S. A. Shehzad and S. Obaidat, Melting heat transfer in the stagnation-point flow of an upper-convected Maxwell (UCM) fluid past a stretching sheet, Int. J. Numer. Methods in Fluid Flows, 68, (2012), 233-243, https://doi.org/10.1002/fld.2503.